Quantifying Local Lung Perfusion and Ventilation Using Correlated SPECT and CT Data

Eugène M.F. Damen, Sara H. Muller, Liesbeth J. Boersma, Roel W. de Boer and Joos V. Lebesque

Departments of Radiotherapy and Nuclear Medicine, The Netherlands Cancer Institute (Antoni van Leeuwenhoek Huis), Amsterdam, The Netherlands

A clinically applicable method for quantifying lung perfusion and ventilation on a subregional (local) scale from SPECT scans in order to estimate local lung function in patients with pre-existing pulmonary disease and to monitor local treatment effects was developed and evaluated. **Methods:** SPECT ^{99m}Tc perfusion and ^{81m}Kr ventilation images were corrected for photon attenuation and scatter effect with a postreconstruction correction method incorporating a variable-effective linear-attenuation coefficient calculated from spatially-correlated CT data. A new algorithm was developed to quantify local ventilation from the SPECT data, which, in contrast with other algorithms, makes no assumptions on ventilation homogeneity over the lung. The quantification procedure was applied to clinical data from patients with a normal lung function and from patients suffering from radiation-induced pulmonary dysfunction. **Results:** The calculated attenuation correction factors on the observed number of counts in the lung range from 2.0 to 3.0 and 2.3 to 3.5 for ^{81m}Kr and ^{99m}Tc, respectively, showing a systematic increase from the diaphragm to the lung apex. As a result of this correction, the values of local perfusion and ventilation differ 10%–15% from values calculated without attenuation correction. The calculated values of the local ventilation are 10%–50% lower than those found by quantification algorithms which assume homogeneous ventilation. **Conclusions:** The methods presented here are robust with respect to uncertainties in the input parameters and yield realistic values for perfusion and ventilation distribution in the lung with an intrinsic accuracy (largely determined by count statistics) of about 10%.

Key Words: quantitative SPECT; attenuation; lung perfusion; lung ventilation

J Nucl Med 1994; 35:784–792

Accurate quantification of lung perfusion and ventilation with a high spatial resolution (subregional or local) using SPECT gives insight into the pathophysiology of local abnormalities. By combining this information with overall lung function parameters, the effect of local abnormalities on the overall lung function can be studied.

At our institution, SPECT perfusion and ventilation scans are used to study the local lung function in relation to the locally absorbed radiation dose of patients receiving radiotherapy for Hodgkin's disease or breast cancer. Accurate quantification of perfusion and ventilation is necessary to compare the post-treatment local lung function with pretreatment values. A detailed description of the first clinical results of this project is given in a separate paper (*1*).

Quantitative use of SPECT data requires correction for photon interactions in the body. Correction algorithms require detailed knowledge of the outline of the patient's body and of the local attenuation coefficient of body tissues (*2,3*). In the thoracic region, the use of a uniform local attenuation coefficient for all tissues is incorrect. Several authors have suggested that (correlated) CT data might be used to determine both the body outline and the local attenuation coefficient (*4–7*), but the use of such a technique is not common in clinical practice.

Conversion of the SPECT data to local ventilation values is a problem in inhomogeneously ventilated lung. SPECT ventilation scans are made with the short-lived radionuclide ^{81m}Kr ($T_{1/2}$ = 13.3 sec), resulting in a nonlinear relationship between observed number of counts and local ventilation (*8*). Most ventilation studies restrict their analysis to planar ventilation images of the lung (*9–11*). The quantification of ventilation from SPECT images has been studied by Klumper and Zwijnenburg (*12*), assuming that the ventilation over the lung is (almost) homogeneous. This assumption is not correct for dysfunctioning lung, e.g., after receiving a radiation dose during treatment for cancer.

The aim of this study is to develop and evaluate a method to accurately quantify local perfusion and ventilation from SPECT scans in order to estimate pulmonary function in different regions of the lung in patients with pulmonary disease and to monitor local treatment effects.

METHODS

Data Acquisition

SPECT ventilation and perfusion scans are made with a dual-head camera (Siemens ZLC-75 Rota II), equipped with medium-

Received Jul. 19, 1993; revision accepted Jan. 20, 1994.

For correspondence or reprints contact: E.M.F. Damen, Department of Radiotherapy, The Netherlands Cancer Institute, Antoni van Leeuwenhoek Huis, Plesmanlaan 121, 1066 CX Amsterdam, The Netherlands.

energy, medium-resolution, parallel-hole collimators. Local perfusion is recorded by intravenously injecting 185 MBq of ^{99m}Tc-labeled macroaggregates which are trapped in the lung capillaries. To record the local ventilation, the patient inhales a mixture of air and ^{81m}Kr through a mouthpiece equipped with low-resistance valves. The patient is supine with arms raised above the head while quietly breathing through the mouthpiece. Attached to the mouthpiece is a pneumotachograph (Jaeger, Würzburg, Germany) used to determine tidal volume (TV), total lung ventilation on expiration (minute volume, $\dot{V}_E$), and expiratory reserve volume (ERV). The ERV is combined with the residual volume (RV) to yield the functional residual capacity (FRC) which is a measure of the average lung volume during tidal breathing. The RV is measured independently using the helium dilution technique with the patient in the same position as during SPECT acquisition.

Perfusion and ventilation images are recorded simultaneously using energy windows with a 10% width centered at the gamma-ray energies of ^{99m}Tc (140 keV) and ^{81m}Kr (190 keV). Following Klumper and Zwijnenburg (*12*), no correction is applied to account for the contribution of scattered 190-keV photons to the 140-keV signal. A total of 60 perfusion and ventilation images of 64 × 64 pixels is recorded at six-degree intervals with an integration time-per-image of 25 sec. Raw images are smoothed using a low-pass filter (9 point, cut-off = 0.25 cycle/pixel) and subsequently reconstructed into 64 transaxial slices (64 × 64 pixels) using a standard filtered backprojection algorithm (Butterworth 4, cut-off = 0.25 cycle/pixel). No attenuation correction is applied to the images during reconstruction. Pixel size and slice thickness are calibrated prior to each SPECT acquisition. They slowly vary in time due to drift in the amplifiers of the system and are both typically 6 mm. The final resolution is largely determined by the use of filters during reconstruction. Using a phantom with cold objects in a uniform background with an activity typical for our patient studies, this resolution has been determined to be approximately 16 mm.

Transaxial CT slices of the thorax with a slice thickness of 8 mm and slice spacing of 10 mm are made on a Somatom Plus scanner (Siemens). A slice consists of 512 × 512 pixels of approximately 0.75 mm^2. Patients are lying in the same position as during SPECT acquisition; the pneumotachograph is used in the same manner as described above. CT imaging of patients is done within 1 wk of SPECT imaging.

Image Correlation

Spatial correlation is necessary to enable the combination of CT and SPECT information. Five markers are used at fixed positions on the patient's skin (crossed radio-opaque catheters for CT and ^{57}Co point sources for SPECT imaging), and the datasets are matched by minimizing the root-mean-square (RMS) distance between corresponding markers. The result is evaluated by superimposing the lung contours from CT and SPECT and checking their relative position. SPECT lung contours are obtained by thresholding with an automatically selected threshold value (the mean pixel value of the edge pixels of the lung volume, defined as the pixels with the highest positive and negative gradient in each line and each column of a gradient image).

Results in 10 patients showed that the mean RMS-distance between the skin markers is 0.6 ± 0.2 cm (1 s.d.) after correlation. The lung contours in SPECT and CT images correlate very well in the lateral parts of the lung (± 0.5 cm (1 s.d.), while the correlation is less near the diaphragm and mediastinum. The uncertainties in contour correlation are largely due to the low resolution of the SPECT images resulting in poorly defined lung contours (*1*).

In the subsequent SPECT data analysis, the lung volume is defined as the volume within the CT contours which can be determined more reliably than the SPECT lung volume.

Attenuation Correction

Our procedure for attenuation correction uses a first-order Chang algorithm (*13*) modified for the use of a variable local linear attenuation coefficient (*4,5*) estimated from the spatially correlated CT data.

The CT images are first converted from 512 × 512 pixels to 128 × 128 pixels. A three-dimensional attenuation map is subsequently created which contains for each voxel of the CT scan the value of the attenuation correction factor, f_{att}, defined as the average attenuation correction factor calculated along lines projecting from the voxel in different directions over 360° (*4,5*). For each voxel crossed by such a projection line, the local linear attenuation coefficient, μ, is calculated from the CT number in Hounsfield Units (HU), using the relationship shown in Figure 1. This relationship is derived by assuming that μ in a voxel is a linear combination of the attenuation coefficients of exactly two types of tissue: either air and muscle or bone and muscle. The attenuation coefficients of these tissues are taken from the literature (*14*). The fraction of each of the two tissues in a voxel depends linearly on the CT scans in that voxel.

Scatter correction is incorporated by reducing the resulting value of μ with a fixed factor, yielding the effective linear attenuation coefficient, μ_{eff} (*15*) (Fig. 1). We determined μ_{eff} in a phantom filled with a homogeneous solution of ^{99m}Tc, resulting in $\mu_{eff} = 0.12$ cm^{-1}, in agreement with the results of other authors (*5,7,15*). The reduction factor is then calculated to be 0.12/0.1545, where 0.1545 cm^{-1} is the tabulated value of the narrow-beam linear attenuation coefficient for ^{99m}Tc in water (*14*). This reduction factor is used for all tissues and for ^{81m}Kr.

Applying this procedure to all CT slices results in a three-dimensional attenuation map where the correction factor for a certain SPECT voxel can be found by tri-linear interpolation.

Perfusion Quantification

The local perfusion (in liter/min) is directly proportional to the local number of technetium atoms trapped in the lung capillaries and thus to the local number of counts observed from a SPECT voxel. The proportionality constant depends on the integration time per image and on several unknown factors such as detector efficiency and patient-camera geometry, which are all constant during the acquisition period. Therefore, the local perfusion in a voxel can be evaluated relative to the total perfusion in the lung and equals the ratio of the number of counts in that voxel-to-the total number of counts in the lung.

When comparing two SPECT scans, a difference in voxel volume may exist, which is taken into account by dividing the calculated perfusion values by the appropriate SPECT voxel volume.

Ventilation Quantification

For ventilation quantification, several assumptions must be made:

1. The lung is regarded as consisting of Z parallel compartments of equal size V_s (constant in time) (Fig. 2), each of which is identified with a SPECT voxel. No distinction is made between compartments where gas diffusion actually takes place and compartments where dead-space ventilation occurs.

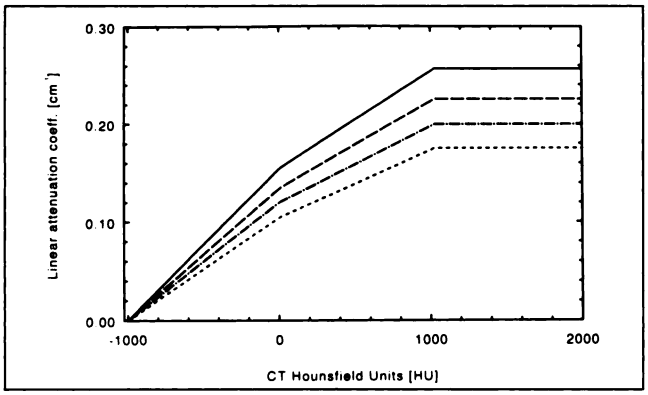

FIGURE 1. Relation between CT HU and linear attenuation coefficient for photon energies of 140 keV (^{99m}Tc, solid line) and 190 keV (^{81m}Kr, dashed). Dashed and dotted lines show the effective linear attenuation coefficient for technetium and krypton, respectively, which includes a correction for photons scattered into the field of view.

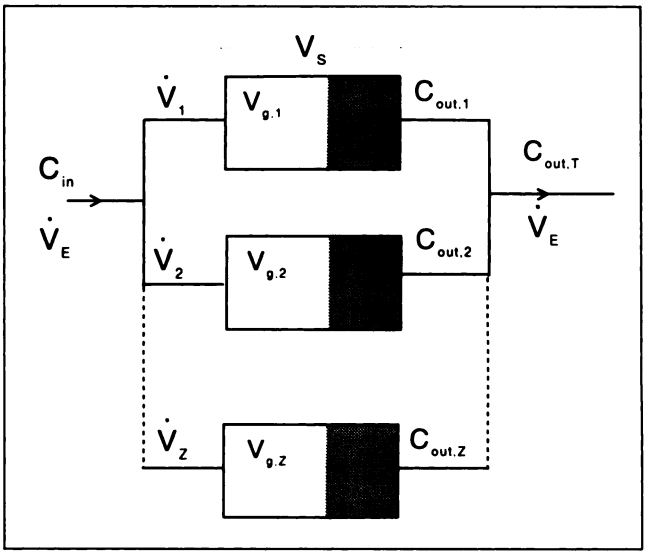

FIGURE 2. Diagram of ventilation model of the lung. See text for an explanation of symbols.

2. The gas-filled sub-volume of a compartment i, $V_{g,i}$ (liter), is equal for all compartments.
3. A steady-state model is assumed (*8,12*), so that the number of ^{81m}Kr atoms in each compartment is constant in time.
4. The krypton concentration in the gas entering a compartment, C_{in} (atoms/liter), is equal for all compartments.
5. Krypton entering a compartment is completely and instantaneously mixed with gas present in the compartment. Hence the krypton concentration in the gas leaving a compartment, $C_{out,i}$, is equal to the krypton concentration in the compartment.

In steady-state, the number of krypton atoms in a compartment is determined by an equilibrium between the arrival of atoms due to ventilation and removal due to ventilation and radioactive decay. The number of counts, M_i, observed in compartment i is proportional to the number of atoms in the compartment. The relation between the compartment ventilation $\dot{V}_i$ and M_i is given by (*8,12*):

$$\dot{V}_i = \frac{\lambda M_i}{gC_{in} - \frac{M_i}{V_{g,i}}}, \qquad \text{Eq. 1}$$

where λ = 3.2 min^{-1} is the decay constant of ^{81m}Kr, and g (counts/atom) is an unknown constant factor which converts the number of atoms to the number of counts. This relation contains three unknown factors: $\dot{V}_i$, $V_{g,i}$ and the count-density in the incoming gas, gC_{in}.

As shown by Klumper and Zwijnenburg (*12*), Equation 1 is also valid for the total lung ventilation only in the case of strictly homogeneous ventilation: $\dot{V}_E = \lambda M_T/(gC_{in} - M_T/V_{g,T})$, where index T refers to total lung. These authors assume that $V_{g,T}$ = FRC and eliminate gC_{in} from Equation 1, which yields an expression for the specific ventilation $R_i = \dot{V}_i/V_{g,i}$ (*12*). Thus, for homogeneous ventilation, R_i can be calculated independently for each voxel.

For inhomogeneous ventilation, gC_{in} can be estimated by requiring that the local ventilation, summed over the total lung volume, equals the total ventilation on expiration $\dot{V}_E$ (minute volume in liters/min) as measured by the pneumotachograph, i.e.:

$$\sum_{i=1}^{Z} \dot{V}_i = \dot{V}_E, \qquad \text{Eq. 2}$$

where $\dot{V}_E$ is the sum of the alveolar ventilation and the dead-space ventilation. Dead-space ventilation in the trachea and bronchi is excluded by use of the CT contours in the analysis of the SPECT data, and by correction of $V_{g,i}$ (see Equation 3 below). The remaining dead-space ventilation is treated as indistinguishable from the alveolar compartments in our parallel model.

$V_{g,i}$ is assumed to be constant, and is estimated as:

$$V_{g,i} = V_g = \frac{FRC + 0.5 \cdot TV - V_d}{Z}, \qquad \text{Eq. 3}$$

where V_d is included to correct for the anatomical dead-space of the trachea and the main bronchi, which is not included in the analysis. This correction volume ($\approx$ 0.05 liter) is small compared to the FRC (typical FRC = 2 liter) and of the same order of magnitude as the accuracy of the FRC measurement.

From Equations 1, 2 and 3, and the requirement that for each voxel the local ventilation must be larger than or equal to zero, a unique solution for gC_{in} can be found. Each value of the local ventilation is directly coupled with gC_{in} and $\dot{V}_E$ and cannot be calculated independently as it is for the homogeneous case (*12*). For strictly homogeneous ventilation, our method is identical to the method of Klumper and Zwijnenburg (*12*).

Similarly, for perfusion $\dot{V}_i$ can be expressed as a fraction of $\dot{V}_E$, and must be normalized to the voxel volume when two ventilation scans are quantitatively compared.

The Influence of Count Statistics

The detection of photons by the gamma camera is a stochastic process theoretically governed by Poisson statistics. The number of observed counts, N, in a SPECT projection will therefore be a sample from a distribution with standard deviation $\sqrt{N}$. Due to the process of backprojecting the data and the use of smoothing and reconstruction filters, the noise in the reconstructed images will be correlated and will deviate from Poisson statistics. The resulting noise level in the reconstructed images generally de-

pends on the activity distribution and on the geometry of the source and the surrounding tissue. To estimate the noise in the reconstructed slices, we used a cylindrical Perspex phantom filled with a homogeneous technetium solution which gave count rates comparable to the mean count rate in our patient studies. The projection data of this phantom was processed using the same filters as for the patient data. The noise in the reconstructed, attenuation-corrected images was estimated to be about 8% of the observed counts in a voxel. Since the count rate is reasonably homogeneous and rarely deviates more than a factor or two from the mean value in most patient studies, this result is representative for the noise in reconstructed lung images.

In the quantification of perfusion, this noise level leads to an uncertainty of 8% (1 s.d.), since perfusion is linearly proportional to the number of counts in a voxel. In the quantification of ventilation, the nonlinearity of the $\dot{V}_i - M_i$ relation results in a bias on the calculated value of the ventilation. The magnitude of this bias depends on the quantity m, the ratio of the count-density in a voxel-to-the count-density in the inspired air ($m = M_i/V_g gC_{in}$). In Appendix B this bias is theoretically calculated for a range of ventilation values.

Practical Implementation and Numerical Stability of Ventilation Quantification

The practical implementation of the ventilation quantification is as follows. Using a first guess for gC_{in}, Equations 1 and 3 are used to calculate R_i ($= \dot{V}_i/V_g$) from M_i. It is then assumed that R_i equals its expectation value $E\{R_i\}$ (Appendix B). Figure B-1 (for an integration interval of $\pm 2.5\sigma$) is subsequently used to find the true ventilation value $R_{t,i}$ (and thus $\dot{V}_{t,i}$), corresponding to this value of $E\{R_i\}$. $\dot{V}_{t,i}$ replaces the original value of $\dot{V}_i$ in Equation 2. If Equation 2 is not fulfilled, a new guess for gC_{in} is made and the whole process is repeated until Equation 2 is met. The ventilation quantification is only considered successful when $m = M_i/V_g gC_{in} \leq 0.83$ ($R_{t,i} \leq 16$ liter/min/liter) for all voxels (see Appendix B).

Using this limit on $R_{t,i}$ also prevents numerical instabilities in the calculation of the ventilation which might occur when the calculated value of gC_{in} is close to the maximum observed count-density in a voxel.

RESULTS

Attenuation Correction Factor

The number of lines used in the calculation of f_{att} is determined by a trade-off between computing time and accuracy. For a transaxial CT slice through the thorax (Fig. 3A), f_{att} in each voxel was calculated using a different number of lines projecting in various directions. The results are displayed as attenuation images in which the grey-level indicates the magnitude of f_{att} (Figs. 3B–F). The use of only four lines (Figs. 3B and C) results in artifacts in the attenuation image, visible as abrupt changes in the attenuation correction factor with a magnitude of up to 15% of the regional average value. Using eight lines reduces the magnitude of the artifacts to about 7% (Figs. 3D and E), while using 16 lines leads to a further reduction to <3% of the regional average value (Fig. 3F). Moreover, the difference in the calculated value of f_{att} using 8 or 16 lines is <3% everywhere.

The calculated values of f_{att} in the lung of a typical patient (Patient P), averaged per SPECT slice, range from 2 to 2.7 for ^{81m}Kr and from 2.3 to 3.1 for ^{99m}Tc (Fig. 4). f_{att} is highest near the lung apices and decreases in the direction of the diaphragm due to the gradual increase of lung tissue (with a low attenuation coefficient) in the photon path. The sharp rise in f_{att} at the bottom of the lung is due to the presence of the diaphragm itself.

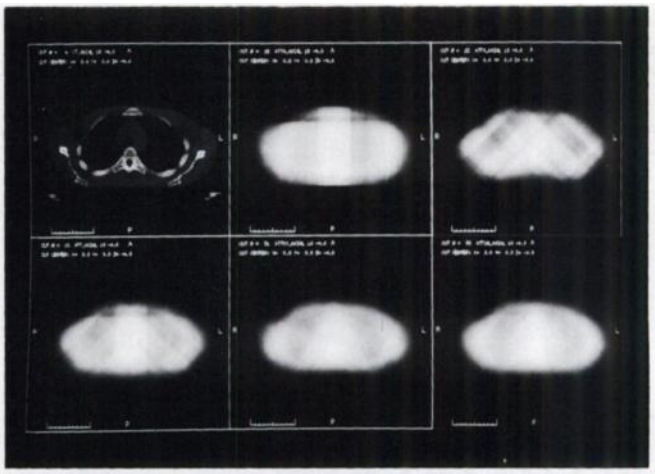

FIGURE 3. Influence of the number and orientation of the lines used in the calculation of attenuation correction factors, f_{att}. (A) (upper left): a transaxial CT slice through the thorax. (B–F) show the same slice, but here the grey-level reflects the magnitude of f_{att}. (B) (upper middle): f_{att} calculated using lines in four directions: up, down, left and right. (C) (upper right): four lines, diagonal directions. (D) (lower left): eight lines, directions of B and C combined. (E) (lower middle): eight lines, directions at intermediate angles. (F) (lower right): 16 lines, directions of D and E combined.

Perfusion and Ventilation Calculation

So far, the data of 23 patients have been calculated both from scans made before and after radiotherapy. The pretreatment data of one of these patients, Patient P, typical for a normal lung function, will be used to illustrate the results of the quantification methods.

The histogram of attenuation-corrected perfusion counts (Fig. 5A) shows a typically broad, slightly asymmetric distribution (mean = 879 ± 342 (1 s.d.) counts/voxel; median = 902 counts/voxel). The calculated local perfusion per unit volume, normalized to the total perfusion and averaged per SPECT slice is at its maximum approximately halfway between the lung apex and the diaphragm (Fig. 6A) and decreases considerably in the direction of the apex. Attenuation correction results in an increase in the calculated average perfusion of 10%–15% near the lung apex and a decrease of the same magnitude near the diaphragm.

The ventilation quantification was successful for all pretreatment scans. For these scans, the histogram of ventilation counts shows a characteristic shape, illustrated in Figure 5A (Patient P). The histogram is asymmetric (mean = 694 ± 265 counts/voxel; median = 724 counts/voxel), showing a clear cut-off in the number of voxels at high count rates.

The ventilation-count histogram of Figure 5A leads to

the relationship between local counts and local ventilation shown in Figure 7 (solid line). The input parameters for this calculation were: $\dot{V}_E$ = 5.48 liters/min; $V_g = 1.9 \times 10^{-4}$ liters. The calculated count density in the inspired air is $gC_{in} = 1.1 \times 10^7$ counts/liter. For this patient, the maximum observed value of m = 0.63, which means that the requirement for a reliable calculation, m ≤ 0.83, is fulfilled. For the highest $\dot{V}$, the bias correction was 3% of the uncorrected $\dot{V}$.

Both the shape of the slice-averaged ventilation distribution in the cranial-caudal direction and the influence of the attenuation correction on this distribution, are comparable to the perfusion results (Fig. 6B).

Most post-treatment scans (17 out of 23) with a moderately inhomogeneous ventilation could be reliably analyzed. However, in 6 out of 23 patients, the post-treatment ventilation analysis was judged to be unreliable (m > 0.83). The shape of the count histogram of these patients differs from the typical shape for normal functioning lung in showing a relatively flat histogram (Patient A, Fig. 5B), indicative of an inhomogeneous ventilation distribution over the lung. To investigate the reason for the failure of the ventilation analysis, we performed several test calculations with slightly modified histograms from Patients P and A. Modifying the histogram at high count rates (where the distribution of counting statistics might lead to unrealistically high values of the number of counts and of the ventilation) did not have any impact on the results. Modifying the "flatness" of the histogram showed that flat histograms increased the value of m considerably (m > 0.83 for the voxels with the highest count rate).

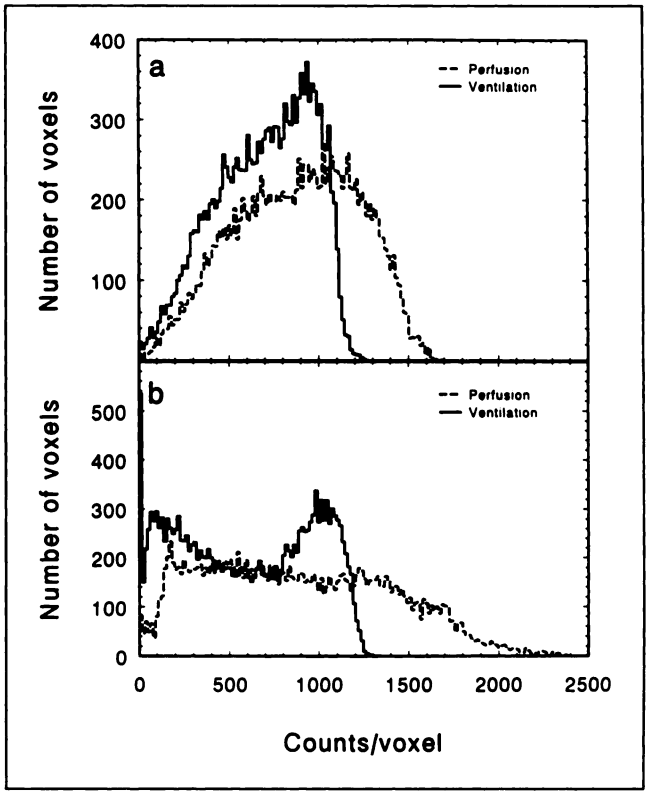

FIGURE 5. Histogram of perfusion and ventilation counts for two patients, illustrating the difference in histograms for normal lung function and dysfunctioning lung. (A) Patient P, normal lung function. (B) Patient A, dysfunctioning lung after irradiation.

Sensitivity Analysis of the Ventilation Quantification

The calculated ventilation distribution depends on the input parameters $\dot{V}_E$, V_g (Equations 2 and 3) and σ (see Appendix B), which are obtained from measurements and have limited accuracy. We repeated the calculation for Patient P with slightly different values for the input parameters in order to determine the solution sensitivity to the uncertainties in these parameters.

The volume of gas expired by the patient is recorded with the pneumotachograph over the whole time-span of SPECT data acquisition. The total ventilation, $\dot{V}_E$, is therefore an accurate mean value during data acquisition with an estimated uncertainty of about 3%. Varying $\dot{V}_E$ with 5% around the measured value results in a maximum variation in the calculated ventilation values of 8% for the few voxels with the highest count rate. For the most abundant count rate (M = 900 counts/voxel, Fig. 5A), the variation is 5%.

The gas-filled volume of the voxels, V_g, is a mean value based on two measurements of FRC and TV using the pneumotachograph. The estimated uncertainty in V_g is about 8%. Variations in V_g of 10%, result in a maximum variation in the ventilation of 6%, again occurring at the highest count rates. For M = 900 counts/voxel, the variation is less than 1%.

The statistical uncertainty in the observed counts in a voxel may vary slightly between different scans, ranging from 6% to 10%, but has no impact on the ventilation distribution.

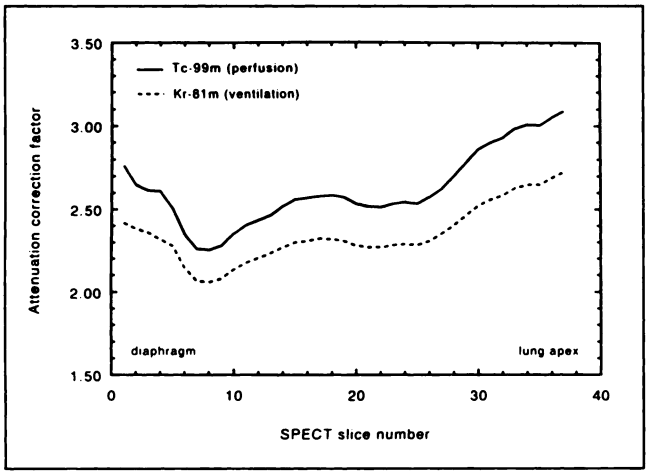

FIGURE 4. Calculated attenuation correction factors for patient P, averaged per SPECT slice for ^{99m}Tc and ^{81m}Kr.

Comparison of Quantification Algorithms

To compare the result of our ventilation algorithm with that of the algorithm of Klumper and Zwijnenburg (*12*) which assumes homogeneous ventilation, we applied the

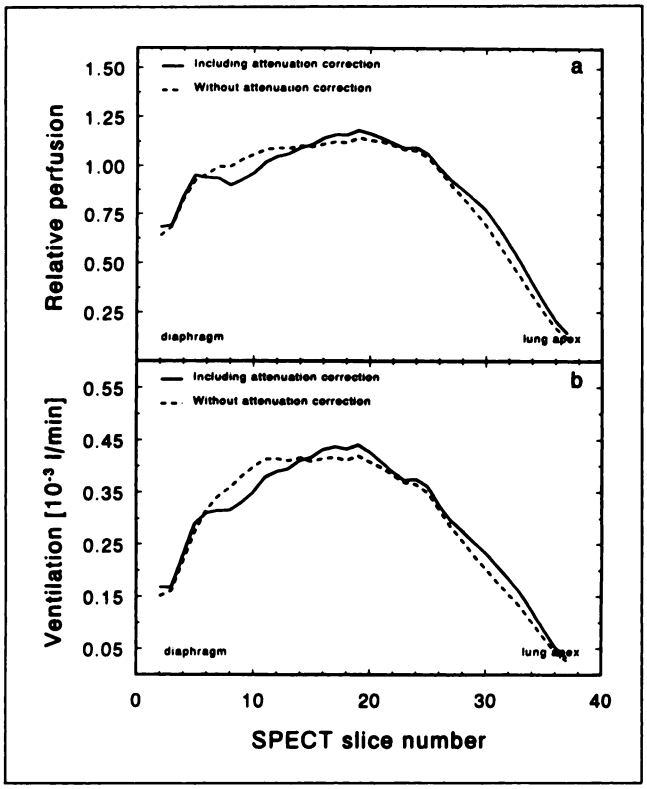

FIGURE 6. Results of quantification of perfusion and ventilation of Patient P and influence of attenuation correction on these results. (A) Perfusion per unit volume, normalized to the total perfusion, averaged per SPECT slice. (B) idem for ventilation, $\dot{V}_i$, averaged per SPECT slice.

latter algorithm to data from two patients: Patient P, who had the lowest observed maximum m (m = 0.63) in our patient group; and Patient C, who had the highest maximum m which still yields reliable results (M = 0.825). For both patients, our ventilation algorithm yields lower values for the ventilation over the whole range of the observed number of counts (Fig. 7). For Patient P, the difference is 16% at the highest count rate and 13% at M = 900 counts/voxel, the count rate occurring with the highest frequency. For Patient C these figures are 50% and 30% (at M = 700 counts/voxel), respectively (Fig. 7).

DISCUSSION

Attenuation Correction

Since local perfusion and ventilation are always related to the total values, the variation of f_{att} over the lung is of greater importance than the absolute value of this parameter. We apply this method to monitor changes in local lung function over a period of months. The method for attenuation correction described in this paper is well-suited for such a differential analysis, but in principle it can be replaced by any other method available now or in the future.

The observed variation of f_{att} in the cranial-caudal direction cannot be reproduced by most commercially available attenuation-correction software, which uses a constant value for the linear attenuation coefficient μ and an elliptical patient contour over the entire thorax. In the case of the comparison of different scans of the same patient (as we do in our study before and after radiotherapy), the local values of f_{att} will be approximately the same in both scans so that the attenuation correction is a second order effect.

Based on the test calculations of the attenuation correction using different numbers of lines, we decided that 16 is the optimum number of lines. The required computation time is still reasonable (about 30 sec computing time per CT slice of 128 × 128 pixels on a VAX3100 workstation), while the 3% uncertainty in the results is small compared to some other sources of error in the quantification procedure (see section on Overall Accuracy).

The results of the attenuation correction may be influenced by the uncertainty of about 0.5 cm (1 s.d.) in the correlation of the SPECT and CT lung surface. Due to the averaging over 16 directions, this small uncertainty will not have a large influence on the results.

In the conversion of the linear attenuation coefficient to an effective attenuation coefficient, a single reduction factor is used for all tissues and for both gamma energies. This procedure gives reasonable results in various phantom studies (*5,7,15*), but may result in a small systematic error in the attenuation correction factors for ^{81m}Kr. Since we only calculate distributions, this uncertainty will not have a large influence on the final results.

Ventilation Quantification

In ventilation quantification, we use $m \leq 0.83$ as a criterion for a reliable result. Whether this condition will be met depends on a combination of factors: the shape of the count-rate histogram and the values of $\dot{V}_E$ and V_g. There is a complicated interrelation between these factors which makes it impossible to predict the outcome of the analysis beforehand.

The gas-filled voxel volume used in this work is a mean value based on the measured FRC and TV. Apart from the

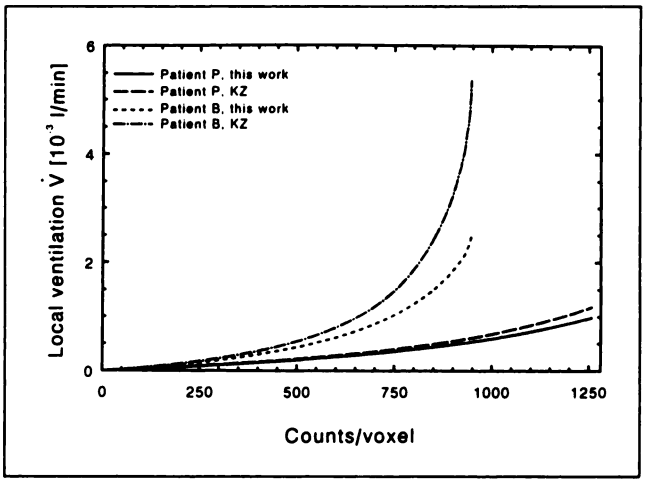

FIGURE 7. Comparison of the results of our ventilation algorithm with those of the algorithm by Klumper and Zwijnenburg (KZ) (*12*). For two patients (Patient P and Patient B), the calculated $\dot{V}$ is given as function of the number of counts per voxel.

uncertainty introduced by measurements with the pneumotachograph (8%), the fixed value of V_g is only a first-order approximation of the real value, since one expects the gas-filled voxel volume to vary depending on the position in the lung. Large deviations leading to errors on local ventilation values are expected in lung regions which contain large vessels (e.g., in the hilar region). However, these regions constitute only a small part of the lung volume and their influence on the calculated ventilation distribution will therefore be small. A gradual decrease in gas-filled volume is expected in the anterior-posterior direction due to the supine position of the patients. This gradual variation will affect the calculated ventilation values only slightly. In the case of a differential analysis, all these effects are of second order.

For about 25% of the ventilation scans made after radiotherapy, the ventilation analysis was judged to be unreliable. As explained in the results section, test calculations show that this failure is probably caused by the flatness of the histogram, i.e., by the inhomogeneity of the ventilation distribution. This would mean that the steady-state model for lung ventilation can no longer be used under these circumstances because it assumes that the lung compartments are rigid structures with a fixed volume ventilated with a flow which is constant in time. Of course, these assumptions are not very realistic but yield reasonable results in cases of moderate air flows and small volume changes. In extreme cases, with both very low and very high flows, a more realistic model is probably needed.

The comparison of our results with those of Klumper and Zwijnenburg (*12*) shows that large deviations between the two algorithms may occur depending on the count distribution in the lung. Even for data from Patient P, who has the most homogeneous ventilation distribution in our patient group, the difference between the two algorithms is considerable. Our results show that the assumption of homogeneous ventilation tends to exaggerate the differences in ventilation over the lung and therefore should be used with care, even in healthy lungs.

Overall Accuracy of the Method

The largest source of uncertainty in the ventilation and perfusion calculation is the 8% (1 s.d.) statistical noise on the images. Additional sources of uncertainty are the attenuation correction (about 3% uncertainty) and the input parameters for the ventilation calculation. Of these ventilation parameters, the gas-filled voxel volume, V_g, is the least certain (estimated uncertainty of 8%). Due to this uncertainty in V_g, an uncertainty <2% occurs in the ventilation calculation of the majority of voxels. Due to the 3% uncertainty on $\dot{V}_E$, a 5% uncertainty occurs for the majority of voxels. Altogether, this yields an overall accuracy for the perfusion calculation method of about 9%, and about 10% for the ventilation. For the voxels with the highest count rates, the uncertainty on the ventilation is a little higher (about 13%).

The figures quoted above refer to the intrinsic uncertainty of the proposed methods and do not indicate their absolute accuracy. It should be realized that these methods are used to quantify the distribution of perfusion and ventilation and not their absolute values. This fact at least partly reduces the influence of systematic uncertainties in the methods. Moreover, the physical and physiological basis of the methods used in this paper, and their demonstrated robustness with respect to input parameters, give confidence that the results are reasonably accurate.

CONCLUSION

We have presented a method to quantify perfusion and ventilation distribution in the lung using ^{99m}Tc perfusion and ^{81m}Kr ventilation SPECT scans combined with a spatially correlated CT scan. The method is well-suited for differential analysis of two SPECT scans made at different times and can be used in clinical practice because patient involvement is minimal and data analysis is not time-consuming. The resulting intrinsic accuracy of the quantification method is about 10%, and the method yields realistic values for relative perfusion and ventilation. In our institution, this method is currently used successfully to monitor local lung function changes after partial irradiation of the lung (*1*).

APPENDIX A

Nomenclature

C_{in}: Concentration of ^{81m}Kr in gas entering a compartment (atoms/liter).

C_{out}: Concentration of ^{81m}Kr in gas leaving a compartment (atoms/liter).

ERV: Expiratory reserve volume (liter).

E{x}: Expectation value of variable x.

f_{att}: Attenuation correction factor, applied to the number of counts in a SPECT voxel.

FRC: Functional residual capacity (liter); FRC = ERV + RV.

g: Efficiency factor for ventilation data acquisition [counts/atom].

HU: Hounsfield unit in CT images.

i: Index referring to individual voxels.

m: Ratio of count-density in a ventilation voxel-to-count-density in the inspired air: $m = M/V_g g C_{in}$.

$\bar{m}$: Mean of normal distribution of m.

M: Attenuation-corrected number of ventilation counts.

P(m): Normal probability distribution of m.

R: Calculated local ventilation per gas-volume, $R = \dot{V}/V_g$ (liter/min/liter).

R_t: True value of the local ventilation per gas-volume (liter/min/liter).

RV: Residual volume (liter).

T: Index referring to the total lung.

TV: Tidal volume (liter).

V_d: Anatomical dead-space in trachea and main bronchi (liter).

V_g: Gas-filled volume of a SPECT voxel (liter).

V_s: Total volume of a SPECT voxel (liter).
$\dot{V}$: Calculated local ventilation (liter/min).
$\dot{V}_E$: Expiratory total ventilation (minute volume) (liter/min).
$\dot{V}_t$: True value of the local ventilation (liter/min).
Z: Number of SPECT voxels within the CT lung volume.
λ: Decay constant of ^{81m}Kr (3.2 min^{-1}).
μ: Narrow-beam linear attenuation coefficient (cm^{-1}).
μ_{eff}: Effective linear attenuation coefficient (cm^{-1}).
σ: Standard deviation of the normal distribution of m.

APPENDIX B

Calculated Ventilation Bias

Due to statistical uncertainty, the nonlinear relationship between the number of ventilation counts and the local ventilation in a voxel will introduce a bias on the calculated ventilation. This bias can be calculated by first rewriting Equation 1 as:

$$R(m) = \lambda \frac{m}{1-m}, \qquad \text{Eq. B1}$$

where $R(m) = \dot{V}/V_g$, $m = M/V_g g C_{in}$. For clarity, the index i is neglected in this appendix.

We assume that the number of counts, and thus parameter m, are normally distributed:

$$P(m) = \frac{1}{\sqrt{2\pi}\,\sigma} \exp\left(-0.5\left(\frac{m-\bar{m}}{\sigma}\right)^2\right), \qquad \text{Eq. B2}$$

The standard deviation of this distribution, σ, is given by:

$$\sigma = 0.08 \cdot \bar{m}, \qquad \text{Eq. B3}$$

where the factor 0.08 is based on the 8% noise level in the reconstructed images. The mean value of m, $\bar{m}$, corresponds to the true value of the ventilation, R_t:

$$\bar{m} = \frac{R_t}{R_t + \lambda}. \qquad \text{Eq. B4}$$

The expectation of R is then given by:

$$E\{R\} = \int_0^1 R(m)P(m)\,dm. \qquad \text{Eq. B5}$$

The bias is defined as the difference between this expectation value and the true value R_t.

Numerical Evaluation of the Bias

By numerically evaluating Equation B5 over an interval around $\bar{m}$, the bias can be calculated for different values of R_t. However, it is not possible to calculate the bias over the whole range of values for m between 0 and 1. As is clear from Equation B1, the value for R(m) will go to infinity when m approaches 1. We therefore define a cut-off value for m, above which R and E{R} cannot be calculated. The range of values of R_t for which a calculation is possible depends on the width of the integration interval and on the cut-off level. In principle, the largest integration interval will give the most accurate results, which are only valid on a small range of values of R_t. We numerically evaluated Equation B5 using three different integration intervals and a cut-off of m = 0.9999 (Fig. B1). When using an interval of $\pm 4\sigma$, cut-off is reached when $\bar{m} = 0.758$, equivalent to $R_t = 10.0$ liter/min/liter, which is too low for practical use. A reduction of the width of the integration interval to $\pm 2.5\,\sigma$ has no large impact on the calculated values of E{R} below $R_t = 10$ liter/min/liter (maximum reduction 3%), but extends the calculation to $\bar{m} = 0.833$, or $R_t = 16$ liter/min/liter (Fig. B1). Reducing the interval even further to $\pm 2.0\,\sigma$ leads to unacceptable large errors in E{R} of up to 8% for $R_t = 10$ liter/min/liter. Based on these test calculations we decided to use the integration interval $\pm 2.5\,\sigma$, and limit all calculations to values of $\bar{m} \leq 0.83$ ($R_t \leq 16$ liter/min/liter).

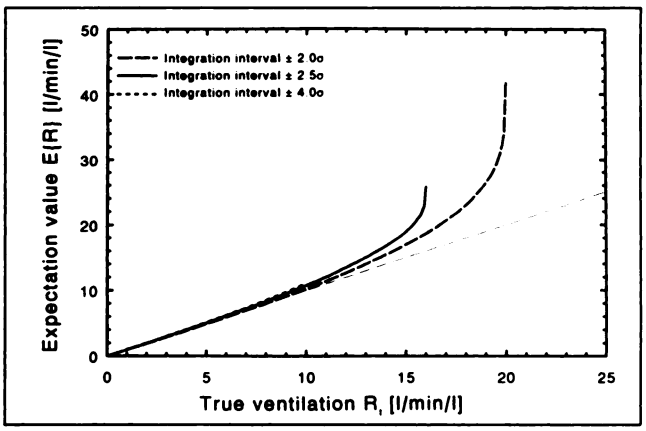

FIGURE B1. The expectation value of the ventilation, E{R}, as function of the true ventilation R_t. E{R} is calculated according to Equation B5 using three different widths of the integration interval and a cut-off value of m = 0.9999. The thin dotted line is for E{R} = R_t.

ACKNOWLEDGMENTS

The authors thank Drs. H. Bartelink and B.J. Mijnheer for critically reading the manuscript; A.A.M. Hart for assistance in preparing Appendix B; Drs. R.A. Valdés Olmos, C.A. Hoefnagel, C.M. Roos, N. van Zandwijk, A. Zwijnenburg and P. Baas for continuous support and useful discussions; M. Koelman, M. Bakker and other nuclear technologists for their contribution to data acquisition and analysis; and T. Minderhoud for providing solutions to many software and hardware problems. This work is supported by the Dutch Cancer Society, grant NKI 90-18.

REFERENCES

1. Boersma LJ, Damen EMF, de Boer RW, et al. A new method to determine dose-effect relations for local lung-function changes using correlated SPECT and CT data. *Radiother Oncol* 1993;29:110–116.
2. Jaszczak RJ, Coleman RE. Single photon emission computed tomography (SPECT): principles and instrumentation. *Invest Radiol* 1985;20:897–910.
3. Parker JA. Quantitative SPECT: basic theoretical considerations. *Semin Nucl Med* 1989;29:3–12.
4. Bailey DL, Hutton BF, Walker PJ. Improved SPECT using simultaneous emission and transmission tomography. *J Nucl Med* 1987;28:844–851.
5. Manglos SH, Jaszczak RJ, Floyd CE, Hahn LJ, Greer KL, Coleman RE. Nonisotropic attenuation in SPECT: phantom tests of quantitative effects and compensation techniques. *J Nucl Med* 1987;28:1584–1591.
6. Fleming JS. A technique for using CT images in attenuation correction and quantification in SPECT. *Nucl Med Commun* 1989;10:83–97.
7. Rowell NP, Glaholm J, Flower MA, Cronin B, McCready VR. Anatomically derived attenuation coefficients for use in quantitative single photon emission tomography studies of the thorax. *Eur J Nucl Med* 1992; 19:36–40.

8. Fazio F, Jones T. Assessment of regional ventilation by continuous inhalation of radioactive krypton-81m. *Br Med J* 1975;3:673–676.
9. Jones T. Theoretical aspects of the use of krypton-81m. In: Lavender PJ, ed. *Applications of krypton-81m, Brit J Radiol special report 15*. 1978:33–37.
10. Amis TC, Jones T. Krypton-81m as a flow tracer in the lung: theory and quantitation. *Bull Europ Physiopath Resp* 1980;16:245–259.
11. Ciofetta G, Silverman M, Hughes JMB. Quantitative approach to the study of regional lung function in children using krypton-81m. *Brit J Radiol* 1980; 53:950–959.
12. Klumper A, Zwijnenburg A. Dual isotope ($^{81}Kr^{m}$ and $^{99m}Tc^{m}$) SPECT in lung function diagnosis. *Phys Med Biol* 1986;31:751–761.
13. Chang L-T. A method for attenuation correction in radionuclide computed tomography. *IEEE Trans Nucl Sci* 1978;NS-25:638–643.
14. Johns HE, Cunningham JR. *The Physics of radiology, 4th edition*. Springfield: Charles C. Thomas;1983:719–740.
15. Harris CG, Greer KL, Jaszczak RJ, Floyd Jr. CE, Edgar CF, Coleman RE. Technetium-99m attenuation coefficients in water-filled phantoms determined with gamma cameras. *Med Phys* 1984;5:681–685.

(continued from page 5A)

FIRST IMPRESSIONS

Hiatal Hernia

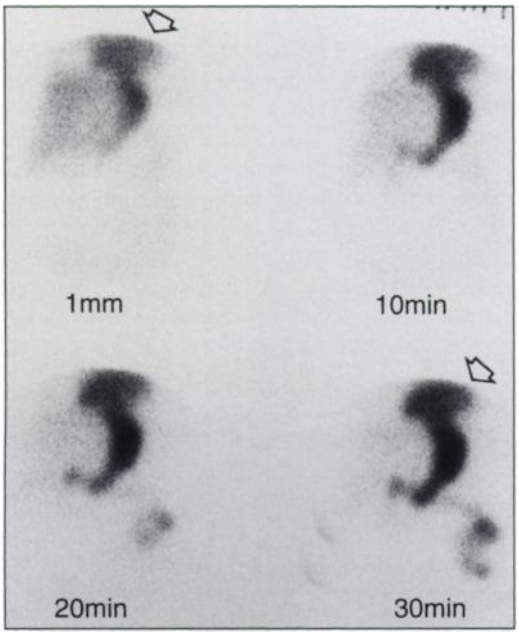

FIGURE 1.

PURPOSE
A 68-yr-old female presented with a history of rectal bleeding. Angiography as well as a ^{99m}Tc-RBC study with heparin challenge were nondiagnostic. A Meckel's scan was performed after angiography demonstrated hypervascularity in the ileal region. The images demonstrate a hiatal hernia (Fig. 1 arrows) which was also seen on the posterior anterior and lateral chest x-rays (Figs. 2-3).

TRACER
Technetium-99m-pertechnetate

ROUTE OF ADMINISTRATION
Intravenous

IMAGING TIME AFTER INJECTION
Immediate and 10-30 minutes

INSTRUMENTATION
Picker LFOV gamma camera

CONTRIBUTORS
Pradeep K. Jacob and Walter H. Williams

INSTITUTION
University of Arizona Health Science Center, Tucson, AZ

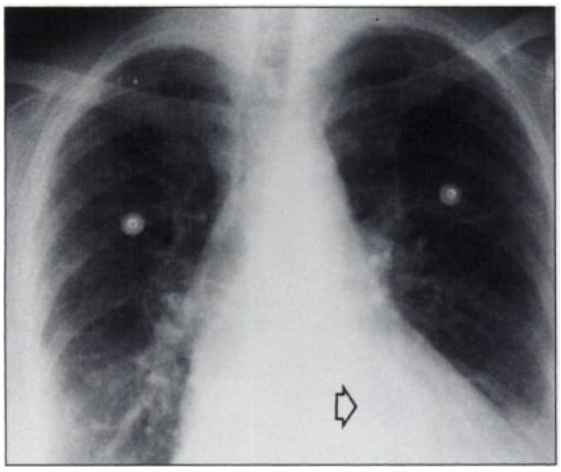

FIGURE 2.

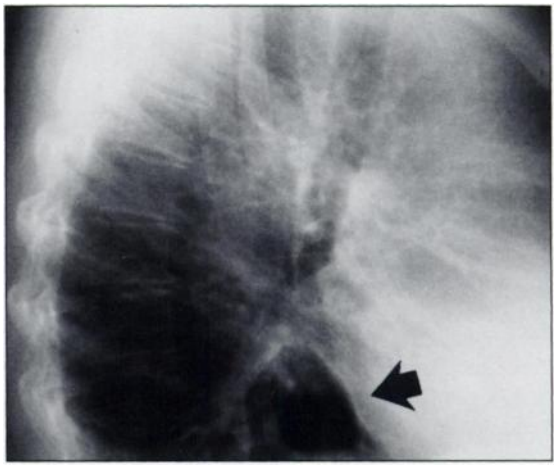

FIGURE 3.